Xu *et al*. *Intell. Robot.* **2025**, *5*(3), 764-81
DOI: 10.20517/ir.2025.39

Intelligence & Robotics

Research Article

Open Access

Data-based dynamic event-triggered attitude control for helicopter with aperiodic denial-of-service attacks

Ye Xu[1], **Huarong Zhao**[1], **Yi Gao**[2], **Hongnian Yu**[3], **Li Peng**[1]

[1]Internet of Things Engineering, Jiangnan University, Wuxi 214122, Jiangsu, China.
[2]Jiangsu Provincial Sensor Network Engineering Technology Research Center, Wuxi Institute of Technology, Wuxi 214121, Jiangsu, China.
[3]School of Computing, Engineering and the Built Environment, Edinburgh Napier University, Edinburgh EH10 5DT, UK.

Correspondence to: Prof. Huarong Zhao, Internet of Things Engineering, Jiangnan University, Wuxi 214122, Jiangsu, China. E-mail: hrzhao@jiangnan.edu.cn; Prof. Hongnian Yu, School of Computing, Engineering and the Built Environment, Edinburgh Napier University, Edinburgh EH10 5DT, UK. E-mail: H.Yu@napier.ac.uk

How to cite this article: Xu, Y.; Zhao, H.; Gao, Y.; Yu, H.; Peng, L. Data-based dynamic event-triggered attitude control for helicopter with aperiodic denial-of-service attacks. *Intell. Robot.* **2025**, *5*(3),764-81. https://dx.doi.org/10.20517/ir.2025.39

Received: 20 Jun 2025 **First Decision:** 22 Jul 2025 **Revised:** 26 Aug 2025 **Accepted:** 1 Sep 2025 **Published:** 28 Sep 2025

Academic Editor: Chen Peng **Copy Editor:** Pei-Yun Wang **Production Editor:** Pei-Yun Wang

Abstract

This paper investigates a dynamic event-triggered model-free adaptive control (MFAC) method for a three-degree-of-freedom helicopter subjected to aperiodic denial-of-service (DoS) attacks to perform attitude control tasks. Firstly, a redefined output is designed to satisfy a quasi-linearization requirement of MFAC theory. Meanwhile, a differential signal is designed to reduce the impact of the redefined output. Then, a dynamic event-triggered strategy is formulated, including a dynamic condition that reduces communication frequencies. Additionally, a DoS attack compensation method has been developed, which effectively mitigates the effects of aperiodic DoS attacks. Moreover, the convergence of the tracking error of the controlled helicopter with the designed method is strictly proven. Finally, simulation results further demonstrate the effectiveness of the designed scheme.

Keywords: Model-free adaptive control, three-degree-of-freedom helicopter, dynamic event-triggered control, denial-of-service attacks

1. INTRODUCTION

Recently, helicopters have garnered considerable attention due to their diverse range of applications in transportation [1], rescue [2], and military operations [3]. Much work has been done on linear/nonlinear controllers applied to helicopters. Among them, Zhao *et al.* designed a three-linear quadratic regulator-based attitude controller [4], Pandey *et al.* proposed a finite-time control strategy [5], and Mokhtari *et al.* designed a robust control scheme based on a third-order dynamic model [6]. Although the most mentioned methods are meaningful, those controller designs are based on a known mathematical model of the vehicle. Since the helicopter is easily influenced by environmental factors, such as wind speeds and humidity [7,8], it is challenging to develop an accurate mathematical model. Hence, it is necessary to investigate a control method that is independent of the dynamics model of the controlled helicopter.

It is noted that data-driven control is a valuable method for solving the above problem, as it does not rely on accurate mathematical models. It instead directly employs the system's input and output data to obtain control strategies. Generally, data-driven control methods are categorized into iterative learning control [9], reinforcement learning control [10], model-free adaptive control (MFAC) [11], and so on. Among them, MFAC methods require fewer parameters to be adjusted and are less sensitive to changes in system parameters. Additionally, iterative learning control relies on repetitive tasks, whereas reinforcement learning control exhibits high computational complexity. In contrast, MFAC is simpler, less computationally burdensome, easier to implement, and more robust, making it more suitable for the nonlinear, dynamic, and real-time control needs of helicopters. Hou first proposed the MFAC method [12], which utilizes only the online input/output data of the controlled system to design the controller. In recent years, as the theory of MFAC has matured and the demand for controlling complex systems in engineering practice has grown, more researchers have applied it to control complex systems in aerospace [13], intelligent driving [14], and energy [15]. For instance, Liu *et al.* proposed an enhanced model-free adaptive attitude control method for a two-wheeled balance vehicle [16], Liu *et al.* proposed an MFAC scheme for a power converter system [17], and Ding *et al.* studied a model-free adaptive sliding mode control method for a quadrotor [18]. Notably, the mentioned results are valuable and significantly contribute to the development of the MFAC theory. However, they did not consider the influence of malicious cyberattacks, which can damage the stability of systems. Therefore, it is worthwhile to investigate the security issues of helicopter systems in the context of malicious cyberattacks.

Generally, cyberattacks can compromise system stability in several ways, including injection attacks [19], replay attacks [20], and denial-of-service (DoS) attacks [21]. Among them, DoS attacks are easy to implement and have become a common threat to network security. Recently, to reduce the impacts of DoS attacks, many meaningful strategies have been developed; for instance, Xiong *et al.* studied a model-free adaptive predictive control method for nonlinear systems with DoS attacks [22], Ma *et al.* designed a model-free adaptive resilient control scheme for multi-agent systems with DoS attacks [23], and Li *et al.* investigated a model-free adaptive iterative learning controller for a nonlinear system against DoS attacks [24]. Although the existing methods are useful, most of them assume that DoS attacks satisfy a periodicity probability model, which is a strict requirement. Generally, it is more practical to investigate whether DoS attacks are aperiodic. Moreover, the methods mentioned above do not sufficiently consider the issue of limited communication resources. Helicopters are usually equipped with lightweight communication devices [25], where communication resources are limited. Hence, it is necessary to investigate a communication strategy to cut the frequency of communication and save communication resources.

It is noted that event-triggered control [26] is a standard solution to communication resource limitation issues. Roughly speaking, the event-triggered methods with different event-triggered conditions can be divided into static event-triggered methods [27] and dynamic event-triggered methods [28]. Recently, several event-triggered MFAC methods have been developed; to illustrate, Yu *et al.* designed a static event-triggered control strategy for nonlinear systems [29], Liu *et al.* studied an anti-interference event-triggered MFAC scheme for intelligent tugs [30], and You *et al.* proposed a static event-triggered background-impulse Kalman filter algorithm for wireless sensor networks [31]. Those studies effectively solve the communication limitation problem and reduce network communication resource consumption. However, most event-triggered MFAC methods rely on fixed

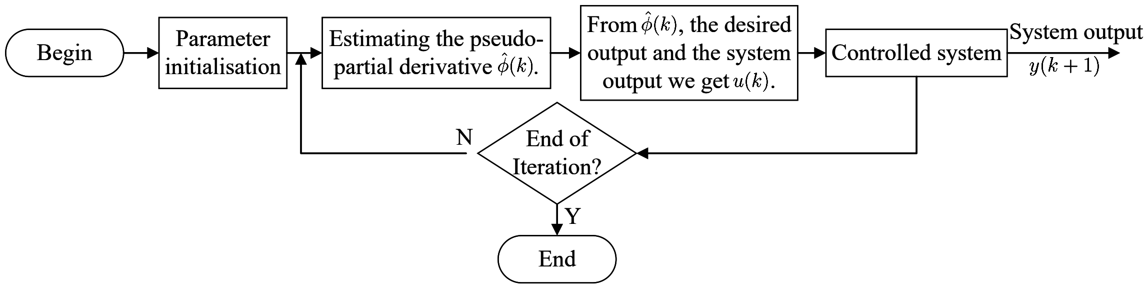

Figure 1. Flowchart of the MFAC algorithm. MFAC: Model-free adaptive control.

thresholds. In contrast, the dynamic event-triggered mechanism has a dynamic event-triggered threshold, which can further reduce the communication burden. Hence, designing a dynamic event-triggered MFAC scheme for Helicopters is meaningful work.

Inspired by the studies mentioned above, this paper examines the attitude control issues of a helicopter subjected to aperiodic DoS attacks and limited communication resources. The main efforts are listed as:

(1) Develop a model-free adaptive attitude control method for the helicopter, which is a data-driven control method. Compared with existing methods[4–6], the dynamics model of the helicopter is no longer needed.

(2) Formulate a forgetting factor-based DoS attack compensation strategy. Compared with the existing method[23], the formulated compensation strategy effectively relieves the impact of aperiodic DoS attacks.

(3) Design a dynamic event-triggered communication mechanism. Compared to static event-triggered methods[29–31], the designed mechanism further reduces the communication frequencies.

The rest of this article is outlined as follows: Section 2 introduces the MFAC method and the controlled system. Section 3 gives the development of the designed method. Section 4 demonstrates the stability of the helicopter converged by the designed scheme. Section 5 demonstrates the effectiveness of the designed method through simulation studies. Finally, Section 6 gives conclusions.

Notations: R, R^{+}, and N^{+} express the set of real numbers, positive real numbers, and positive integers. $A\backslash B$ represent the set belongs to the set A but not the set B. $\text{sign}(\cdot)$ denotes a sign function. $\|\cdot\|$ indicates a two-norm function. Besides, $k \in 1, 2, \ldots$ stands for the time instant.

2. PRELIMINARY AND PROBLEM FORMULATION

2.1. MFAC method

The core idea is to build an equivalent dynamic linearized model at each operating point, and to estimate the pseudo-partial derivative (PPD) parameters of the system online from the input and output data of the controlled system. In this case, the PPD parameter is a mathematical concept. It is a parameter that approximates the relationship between the system's input and output data to establish a dynamic linearization model, such as compact form dynamic linearization (CFDL), partial form dynamic linearization (PFDL), and full form dynamic linearization (FFDL). Subsequently, a MFAC method is proposed based on the established dynamic linearization model. The flowchart of the control algorithm is shown in Figure 1[32]. For complete theoretical foundations (e.g., stability proofs, algorithmic variants), refer to Refs.[33] and[34].

Considering a single-input single-output nonlinear system[35] satisfies that

$$y(k+1) = f(y(k), ..., y(k-n_y), u(k), ..., u(k-n_u)) \tag{1}$$

where $f(\cdot)$ is an unknown nonlinear function. $y(k) \in R$ and $u(k) \in R$ denote the system input and output, respectively. n_y and n_u are unknown positive orders of the output and input, respectively. Besides, we consider the following assumptions.

Assumption 1[36] The partial derivative of $f(\cdot)$ with respect to $u(k)$ is continuous.

Assumption 2[37] The system, given in Equation (1), satisfies the generalized Lipschitz condition, if $|\Delta u(k)| = |u(k) - u(k-1)| \neq 0$, then it is obtained that $|y(k+1) - y(k)| \leq b|u(k) - u(k-1)|$, where b is a positive constant.

Remark 1 Assumption 1 is a common condition of nonlinear systems. Assumption 2 is a restriction on the upper bound of the system output change rate. More deities of Assumptions 1 and 2 can be found in the reference[38].

Lemma 1[39] If Equation (1) satisfies Assumptions 1-2 and $\Delta u(k) \neq 0$, there exists a time-varying parameter called PPDs $\phi(k)$, such that Equation (1) is transformed into

$$\Delta y(k+1) = \phi(k)\Delta u(k) \tag{2}$$

where $\phi(k)$ is bounded and satisfies $|\phi(k)| \leq b$.

Assumption 3[40] The sign of the PPD parameter remains unchanged for all k and satisfies $\phi(k) > \varepsilon > 0$ or $\phi(k) < -\varepsilon, \forall k$. Without loss of generality, we assume $\phi(k) > \varepsilon$, where ε is a small positive number.

Remark 2 Assumption 3 implies that the system's output does not decrease when the input increases, also called a quasi-linearization requirement[41].

2.2. System descriptions

The three-degree-of-freedom helicopter features two direct current motors, one mounted at each end of a rectangular frame, which drive two propellers. The helicopter's attitude is controlled by the thrust forces F_b and F_f generated by the two propellers. Note that the system is underactuated with only two control forces and three degrees of freedom. Moreover, the helicopter has three degrees of freedom: elevation angle ε, heading angle ψ, and pitch angle θ. The nonlinear model of the three-degree-of-freedom helicopter attitude control subsystem is given as

$$\begin{aligned} J_x\ddot{\varepsilon} &= K_f(V_f + V_b)L_a\cos\theta - T_g\cos\varepsilon \\ J_y\ddot{\psi} &= T_g L_a \sin\theta \\ J_z\ddot{\theta} &= K_f(V_f - V_b)L_h \end{aligned} \tag{3}$$

where V_f and V_b are the two voltages of the helicopter's motors. J_x, J_y, and J_z are the moments of inertia of the elevator, heading, and pitch axes, respectively. T_g is the equivalent gravitational moment of the pitch axis, L_h is the distance from the pitch axis to each motor, L_a is the distance from the heading axis to the helicopter fuselage, and K_f is the propeller thrust constant.

Remark 3 When helicopters are performing smooth hovering or slow attitude adjustment tasks, their pitch angle is usually in a small range. At this point, the Taylor series expansion of $\sin\theta$ is performed: $\sin\theta = \theta - \frac{\theta^3}{6} + \frac{\theta^5}{120} - \cdots$. When $\theta \leq 0.1$ rad, the absolute value of the higher order terms of the third order and above is much smaller than θ itself, such as $\frac{\theta^3}{6} \leq \frac{0.1^3}{6} \approx 1.67 \times 10^{-4}$. For large-angle scenarios, the enhanced nonlinear coupling will lead to the failure of the approximation, and this issue will be the main focus of the next phase of research.

Then it is obtained that $\sin(\theta(k)) \approx \theta(k)$. Let $V_f + V_b = V_1$ and $V_f - V_b = V_2$. Hence, Equation (3) is discretized as

$$\begin{cases} \varepsilon(k+1) = \varepsilon(k) + T_s r_\varepsilon(k+1) \\ r_\varepsilon(k+1) = r_\varepsilon(k) + (T_s K_f V_1(k)\times \\ L_a \cos(\theta(k)) - T_s T_g \cos(\varepsilon(k)))/J_x) \end{cases}$$
$$\begin{cases} \psi(k+1) = \psi(k) + T_s r_\psi(k+1) \\ r_\psi(k+1) = r_\psi(k) + T_s T_g L_a \theta(k)/J_y \end{cases} \tag{4}$$
$$\begin{cases} \theta(k+1) = \theta(k) + T_s r_\theta(k+1) \\ r_\theta(k+1) = r_\theta(k) + T_s K_f V_2(k) L_h / J_z \end{cases}$$

where T_s denotes the system sampling time. Moreover, $r_\varepsilon(k)$, $r_\psi(k)$, and $r_\theta(k)$ denote the angular velocities of elevation angle, heading angle, and pitch angle, respectively.

Remark 4 From the discrete-time model of the helicopter, given in Equation (4), it is found that the angular velocity of $\psi(k)$ is positively correlated with $\theta(k)$, which means that $\psi(k)$ will continue to change when $\theta(k) \neq 0$; that is, $\theta(k)$ must eventually converge to 0 for $\psi(k)$ to stabilize.

Remark 5 Although the dynamics models of the helicopter are discussed in Equations (3) and (4), those models are only uncertainties and are employed to demonstrate the relationship between input data and output data of the controlled helicopter. It should be noted that the mentioned models are no longer required when designing the controller. This paper aims to design a data-driven control method for the helicopter to realize attitude control.

2.3. Aperiodic DoS attacks

DoS attacks aim to break system stability by blocking data transmission. Figure 2 illustrates a schematic diagram of the aperiodic DoS attack behavior. The nth DoS attack interval is defined as $[T_n^{\text{on}}, T_n^{\text{off}})$, where T_n^{on} and $T_n^{\text{off}} \in R^+$ are the start instant and the end instant of DoS attacks, respectively. The joint value of the DoS attacks for $k \in R^+$ in the interval $[0, k]$ is

$$\upsilon_a(0,k) = \left\{ \bigcup_{n \in R^+} [T_n^{on}, T_n^{off}) \right\} \bigcap [0,k] \tag{5}$$

Then, the time interval without DoS attacks is given by

$$\upsilon_s(0,k) = [0,k] \backslash \upsilon_a(0,k) \tag{6}$$

Assumption 4[42] Defining $|\upsilon_a(0,k)|$ as the total time interval with DoS attacks in $[0, k]$, it satisfies that

$$|\upsilon_a(0,k)| \leq \upsilon_0 + \frac{k}{\tau_a} \tag{7}$$

where $\tau_a > 1$ and $\upsilon_0 \geq 0$ are constants to be determined.

Remark 6 Assumption 4 implies that the total duration of DoS attacks is bounded. In addition, the role of υ_0 is to consider the situation at the beginning of the DoS attacks. τ_a is a parameter that affects the frequency of the DoS attack. The frequency of the DOS attack is $\frac{1}{\tau_a}$.

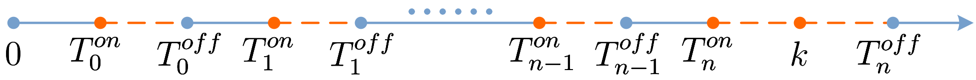

Figure 2. Scheme of DoS attacks. DoS: Denial-of-service.

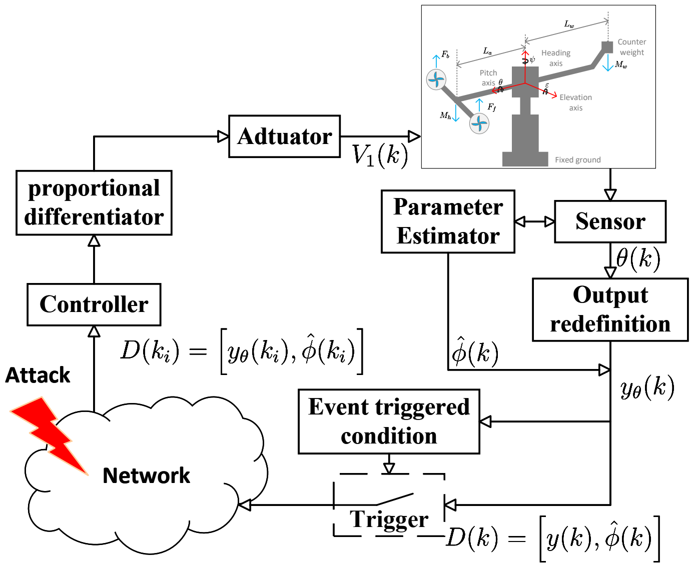

Figure 3. The schematic diagram of the formulated method.

2.4. Problem statement

The primary objective of this paper is to propose a data-driven, dynamic event-triggered attitude control method for helicopters to facilitate the implementation of attitude control tasks. To improve the control performance and resource utilization efficiency, it faces the following key challenges:

(1) **Quasi-linearization Issue**: The relationship between input and output data of the controlled helicopter does not satisfy the quasi-linearization requirement, which is a basic requirement for MFAC theory.

(2) **Aperiodic DoS Attack Issue**: The controlled helicopter system is subject to aperiodic DoS attacks, leading to the controller being unable to receive the feedback data.

(3) **Limited Communication Resources**: Generally, due to the restrictions on size and quality, helicopters are equipped with a lightweight communication device, which will cause communication jamming.

To summarize, this paper proposes a data-driven control scheme based on the MFAC theory, addressing the issues of aperiodic DoS attacks and limited communication resources.

3. CONTROLLER DESIGN AND ANALYSIS

The schematic diagram of the formulated scheme is shown in Figure 3, which mainly includes a three-degree-of-freedom helicopter, output redefiner, trigger, and controller. The trigger keeps the value of the previous moment when the event-triggered condition is not met until the event is triggered, that is, $u_i(k) = u_i(k_i)$ with $k_i < k < k_{i+1}$, where k_i denotes the last event-triggered instant.

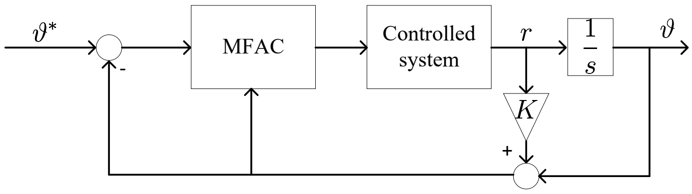

Figure 4. The schematic diagram of the formulated method.

3.1. Output redefinition

It should be pointed out that the attitude angles of the helicopter have a characteristic of suddenly changing to the opposite extreme value (for example, 180° jumps to −180°) when approaching the critical value. Therefore, the three-degree-of-freedom helicopter attitude control model given in Equation (4) does not satisfy Assumption 3. By analyzing the dynamic characteristics of the helicopter system and incorporating the quasi-linearization requirements of the MFAC theory, a redefined output is designed.

This article reconstructs the output signal using the angles and angular velocities of the three attitude angles and proves that the redefined output and the input satisfy Assumption 3. The output signal is redefined as

$$z(k) = \vartheta(k) + Kr(k) \tag{8}$$

where $\vartheta(k)$ and $r(k)$ represent the angle and angular velocity, respectively. $K \geq K_{min}$ is the redefined angular velocity gain, and K_{min} is a certain least positive number.

Redefine the reference signal for the system output as

$$z^*(k) = \vartheta^*(k) + Kr^*(k) \tag{9}$$

where $\vartheta^*(k)$ and $r^*(k)$ represent the desired angle and angular velocity, respectively. At the stabilization point, there exists $z^*(k) = \vartheta^*(k) + Kr^*(k) = \vartheta^* + Kr^* = \text{const}$, where ϑ^* represents the desired heading angle, and the desired angular velocity r^* is always zero. Assumption 3 is satisfied by choosing an appropriate parameter K such that $K * r$ continues to increase during attitude angle jumps, thus ensuring that the control output z also increases.

As shown in Figure 4, the system introduces the angular velocity signal into the outer loop feedback system by redefining the output. This reflects the combined effect of interference on heading and angular velocity in a prompt manner. Thus, the controller can be adjusted more quickly to improve the system's anti-interference capability and dynamic response speed. Relevant details can be found in[43].

Theorem 1 The redefined output Equation (8) satisfies Assumption 3 when $K \geq K_{min} = \max(K_\varepsilon, K_\lambda, K_\rho)$ with $K_\varepsilon = \frac{2\pi J_x}{T_s K_f L_a \cos(\theta(k))\Delta V_1(k) - T_s T_g \cos(\varepsilon(k)))} - T_s$, $K_\lambda = \frac{2\pi J_y}{T_s T_g L_a \theta(k)} - T_s$, and $K_\rho = \frac{2\pi J_z}{T_s K_f L_h V_2(k)} - T_s$. At the same time, if set $z(k) = z^*(k)$, it is obtained that $\vartheta(k)$ converges asymptotically to $\vartheta^*(k)$.

Proof 1 The output increment satisfies:

$$\begin{aligned} \Delta z(k) &= \Delta\vartheta(k) + K\Delta r(k) \\ &= (\frac{\Delta\vartheta(k) + K\Delta r(k)}{\Delta u(k)})\Delta u(k) \end{aligned} \tag{10}$$

Supposing $\Delta u(k) > 0$, take elevation angle $\varepsilon(k)$ as an example. Then, consider an extreme case, the angle jumps from 180° to 180°. Under this circumstances, $\varepsilon(k) = -2\pi$. Substituting Equation (4) into $\Delta z(k+1)$

yields

$$\begin{aligned}\Delta z(k+1) &= \Delta\varepsilon(k+1) + K\Delta r_\varepsilon(k) \\ &= \Delta\varepsilon(k) + (T_s+K)\Delta r_\varepsilon(k+1) \\ &= \Delta\varepsilon(k) + (T_s+K)(\frac{T_sK_fL_a\cos(\theta(k))}{J_x}\Delta V_1(k) - \frac{T_sT_g\cos(\varepsilon(k)))}{J_x})\end{aligned} \tag{11}$$

In actual systems, a dead zone exists in the controller's output, allowing the helicopter to take off. This means that when $u(k) > u_{min} > 0$, $\Delta r(k) > 0$ must hold. Thus, Equation (11) is transformed into

$$\begin{aligned}&\Delta\varepsilon(k) + (T_s+K)(\frac{T_sK_fL_a\cos(\theta(k))}{J_x}\Delta V_1(k) - \frac{T_sT_g\cos(\varepsilon(k)))}{J_x}) \\ &\geq -2\pi + (T_s+K)(\frac{T_sK_fL_a\cos(\theta(k))}{J_x}\Delta V_1(k) - \frac{T_sT_g\cos(\varepsilon(k)))}{J_x}) \\ &\geq 0\end{aligned} \tag{12}$$

Obviously, if $K \geq K_\varepsilon = \frac{2\pi J_x}{T_sK_fL_a\cos(\theta(k))\Delta V_1(k) - T_sT_g\cos(\varepsilon(k)))} - T_s$, Equation (11) holds. Similarly, $K \geq K_\lambda = \frac{2\pi J_y}{T_sT_gL_a\theta(k)} - T_s$ and $K \geq K_\rho = \frac{2\pi J_z}{T_sK_fL_hV_2(k)} - T_s$ ensure that Assumption 3 can be satisfied. In summary, if $K \geq \max(K_\varepsilon, K_\lambda, K_\rho)$, it is concluded that Equation (8) satisfies Assumption 3. When $\Delta u(k) < 0$, the same reasoning holds.

Substituting Equations (8) and (9) into $z(k) = z^*(k)$, we have

$$\vartheta(k) - \vartheta^*(k) + K(r(k) - r^*(k)) = 0 \tag{13}$$

Considering

$$\begin{cases} r(k) = \frac{\vartheta(k)-\vartheta(k-1)}{T_s} \\ r^*(k) = \frac{\vartheta^*(k)-\vartheta^*(k-1)}{T_s}\end{cases} \tag{14}$$

where T_s is the sampling period.

Substituting Equation (14) into Equation (13) yields

$$\frac{K}{T_s}(\vartheta(k) - \vartheta(k-1) - \vartheta^*(k) + \vartheta^*(k-1)) + \vartheta(k) - \vartheta^*(k) = 0 \tag{15}$$

Defining $e_\vartheta(k) = \vartheta(k) - \vartheta^*(k)$, Equation (15) becomes

$$e_\vartheta(k) = \frac{K}{K+T_s}e_\vartheta(k-1) \tag{16}$$

According to Equation (16), $e_\vartheta(k)$ converges to 0 as k tends to infinity, that is, $\vartheta(k)$ converges to $\vartheta^*(k)$ asymptotically. Based on the above calculation, Theorem 1 is proved.

It should be pointed out that although the control error converges when the design parameter K takes an appropriate value, its value affects the system performance. To solve this problem, we add a differential signal at the input of the system, and the control input becomes

$$u_d(k) = K_d\frac{(u(k) - u(k-1))}{T_s} + K_{pd}u(k) \tag{17}$$

where K_d and K_{pd} is the differential gain and proportional gain, respectively. T_s is a sampling period.

3.2. DoS attack compensation algorithm

Unmanned helicopters rely on network communications to send data to interact with ground terminals or other aircraft. For example, when performing missions, they need to upload flight attitude and position data and receive control commands in real-time. This exposes them to the risk of cyberattacks, especially DoS attacks, which are easy to implement. Hence, designing a DoS attack compensation algorithm for the helicopter is meaningful work.

DoS attacks can cause delays, data loss and interruption of communication between unmanned helicopters and ground control stations. These attacks consume network bandwidth and send large numbers of invalid packets. These issues significantly affect flight control, rendering it impossible to execute control commands promptly or provide accurate feedback on flight attitude data. This paper presents a compensation algorithm based on MFAC that aims to counteract the effects of DoS attacks. This algorithm compensates for the effects of a DoS attack on the communication system by dynamically adjusting control inputs to ensure flight stability and control accuracy.

Take the elevation channel as an example, a DoS attack compensation algorithm [44] is designed as

$$u_a(k) = u_a(k-1) + \bar{\varrho}(k)\beta^m \Delta u_a(k_{cr}) + \varrho(k)\frac{\sigma_a \hat{\phi}_a(k_i)}{\alpha_a + |\hat{\phi}_a(k_i)|^2}(y_\varepsilon^*(k+1) - y_\varepsilon(k_i)) \tag{18}$$

where $\beta \in (0,1)$ is a compensation parameter for DoS attacks. $\varrho(k) = 0$ when the system is under DoS attack, $\varrho(k) = 1$ when the system is not under DoS attack. m is the number of consecutive DoS attacks. $\Delta u_a(k_{cr}) = u_a(k_{cr}) - u_a(k_{cr}-1)$, k_{cr} is the moment of the latest DoS attack, and

$$\bar{\varrho}(k) = \begin{cases} 1, \ if \ \varrho(k) = 0 \\ 0, \ if \ \varrho(k) = 1 \end{cases} \tag{19}$$

3.3. Dynamic event-triggered mechanism

Notably, the developed scheme is based on a continuous network communication condition. It should be pointed out that the helicopter's network resources are limited. To save communication resources, we introduce a dynamic event-triggered mechanism. Defining the set of event-triggered instants is $\{k_i, i = 0, 1, \ldots\}$. Then, a dynamic event-triggered function is developed as

$$g(k) = \frac{1}{\nu}|\upsilon(k)| + \omega - |e(k)| \tag{20}$$

where ν and ω are positive constants. $e(k) = y^*(k) - y(k)$ is the tracking error. $y^*(k) = \vartheta^*(k) + Kr^*(k)$, $y(k) = \vartheta(k) + Kr(k)$. $\upsilon(k)$ represents the dynamic variable satisfying

$$\upsilon(k+1) = \varphi\upsilon(k) + \omega - |e(k)|, \upsilon(1) = \upsilon_0 \tag{21}$$

where $\varphi > 0$, and υ_0 is the initial value of $\nu(k)$.

Then, an event-triggered condition is formulated as

$$k_{i+1} = \inf\left\{k \in N^+ | k > K_i, g(k) < 0\right\}. \tag{22}$$

When $g(k) \geq 0$, that is, $|e(k)| \leq \frac{1}{\nu}|\upsilon(k)| + \omega$, the control signal stops updating. When $g(k) < 0$, that is, $|e(k)| > \frac{1}{\nu}|\upsilon(k)| + \omega$, the system triggers communication and updates the control signal.

Remark 7 As ν tends to infinity, the event triggering strategy degenerates into a static triggering strategy. Compared with the static event triggering strategy with a fixed threshold, a dynamic triggering strategy can adaptively adjust the triggering threshold according to the system state $|e(k)|$, thus further reducing the number of communications and the communication load.

3.4. Dynamic event-triggered MFAC approach development

Considering that the helicopter is an underactuated system, the first equation in Equation (4) is treated as a subsystem with control input $V_1(k)$, and the second and third equations in Equation (4) are treated as another subsystem with control input $V_2(k)$. Hence, the designed MFAC scheme includes two parts.

Combining Equations (17)-(22) and the DoS attack mechanism, the improved control scheme can be summarized as

$$\begin{cases} \hat{\phi}_a(k) = \hat{\phi}_a(k-1) + \frac{\eta_a \Delta u_a(k-1)}{\mu_a + (\Delta u_a(k-1))^2} \times (\Delta y_\varepsilon(k) - \hat{\phi}_a(k-1)\Delta u_a(k-1)) \\ \hat{\phi}_a(k) = \hat{\phi}_a(1), \text{ if } \operatorname{sign}(\hat{\phi}_a(k)) \neq \operatorname{sign}(\hat{\phi}_a(1)) \text{or } |\hat{\phi}_a(k)| \leq \delta \text{ or } |\Delta u_a(k-1)| \leq \delta \\ u_a(k) = u_a(k-1) + \varrho(k) \frac{\sigma_a \hat{\phi}_a(k_i)}{\alpha_a + |\hat{\phi}_a(k_i)|^2} (y_\varepsilon^*(k+1) - y_\varepsilon(k_i)) \\ V_1(k) = K_a \frac{(u_a(k) - u_a(k-1))}{T_s} + K_{pa} u_a(k) \end{cases} \tag{23}$$

where

$$\varrho(k) = \begin{cases} 1, k \in [T_{n-1}^{\text{off}}, T_n^{\text{on}}) \\ 0, k \in [T_n^{\text{on}}, T_n^{\text{on}}) \end{cases} \tag{24}$$

Moreover, $y_\varepsilon^*(k+1) = \varepsilon^*(k+1) + K_\varepsilon r_\varepsilon^*(k+1)$, $y_\varepsilon(k) = \varepsilon(k) + K_\varepsilon r_\varepsilon(k)$, $\Delta y_\varepsilon(k) = y_\varepsilon(k) - y_\varepsilon(k-1)$, η_a, and σ_a are step factors. Moreover, μ_a and α_a are weighting factors. ε^* and r_ε^* are the expected values of the elevation angle and corresponding angular velocity, respectively. K_ε is the angular velocity gain of ε. K_a is the differential gain. K_{pa} is the proportional gain.

The heading and pitch channels are single-input and two-output nonlinear systems. Similarly to the designed method in Equation (23), the controller $V_2(k)$ is designed as

$$\begin{cases} \begin{bmatrix} \hat{\phi}_{c1}(k) \\ \hat{\phi}_{c2}(k) \end{bmatrix} = \begin{bmatrix} \hat{\phi}_{c1}(k-1) \\ \hat{\phi}_{c2}(k-1) \end{bmatrix} + \frac{\eta_c \Delta u_c(k-1)}{\mu_c + (\Delta u_c(k-1))^2} \times (\begin{bmatrix} \Delta y_\psi(k) \\ \Delta y_\theta(k) \end{bmatrix} - \begin{bmatrix} \hat{\phi}_{c1}(k-1) \\ \hat{\phi}_{c2}(k-1) \end{bmatrix} \Delta u_c(k-1)) \\ \begin{bmatrix} \hat{\phi}_{c1}(k) \\ \hat{\phi}_{c2}(k) \end{bmatrix} = \begin{bmatrix} \hat{\phi}_{c1}(1) \\ \hat{\phi}_{c2}(1) \end{bmatrix}, \text{if} \begin{bmatrix} \operatorname{sign}(\hat{\phi}_{c1}(k)) \\ \operatorname{sign}(\hat{\phi}_{c2}(k)) \end{bmatrix} \neq \begin{bmatrix} \operatorname{sign}(\hat{\phi}_{c1}(1)) \\ \operatorname{sign}(\hat{\phi}_{c2}(1)) \end{bmatrix} \\ \text{or} \begin{bmatrix} |\hat{\phi}_{c1}(k)| \\ |\hat{\phi}_{c2}(k)| \end{bmatrix} \leq \begin{bmatrix} \delta \\ \delta \end{bmatrix} \text{or} |\Delta u_c(k-1)| \leq \delta \\ u_c(k) = u_c(k-1) + \varrho(k) \dfrac{\sigma_c \begin{bmatrix} \hat{\phi}_{c1}(k_i) \\ \hat{\phi}_{c2}(k_i) \end{bmatrix}^T}{\alpha_c + \begin{bmatrix} \hat{\phi}_{c1}(k_i) \\ \hat{\phi}_{c2}(k_i) \end{bmatrix}^T \begin{bmatrix} \hat{\phi}_{c1}(k_i) \\ \hat{\phi}_{c2}(k_i) \end{bmatrix}} \times (\begin{bmatrix} y_\psi^*(k+1) - y_\psi(k_i) \\ y_\theta^*(k+1) - y_\theta(k_i) \end{bmatrix}) \\ V_2(k) = K_c \frac{(u_c(k) - u_c(k-1))}{T_s} + K_{pc} u_c(k) \end{cases} \tag{25}$$

where $y_\psi^*(k+1) = \psi^*(k+1) + K_\psi r_\psi^*(k+1)$, $y_\psi(k) = \psi(k) + K_\psi r_\psi(k)$, $\Delta y_\psi(k) = y_\psi(k) - y_\psi(k-1)$, $y_\theta^*(k+1) = \theta^*(k+1) + K_\theta r_\theta^*(k+1)$, $y_\theta(k) = \theta(k) + K_\theta r_\theta(k)$, and $\Delta y_\theta(k) = y_\theta(k) - y_\theta(k-1)$. η_c and σ_c are step factors. μ_c and α_c are weighting factors. ψ^* and r_ψ^* are the expected values of the heading angle and corresponding angular velocity, respectively. θ^* and r_θ^* are the expected values of the pitch angle and angular velocity, respectively. K_ψ and K_θ are the angular velocity gains for ψ and θ, respectively. K_c is the differential gain, and K_{pc} is the proportional gain.

4. STABILITY ANALYSIS

Lemma 2[42] When the condition Equation (22) does not hold and without DoS attacks, $\nu > 0$, $\varphi > 0$, and $0 < \frac{1}{\nu} + \varphi < 1$, we have

$$\{\upsilon(k) \| \upsilon(k)| \leq \frac{2\omega}{1 - (\varphi + \frac{1}{\nu})}\} \tag{26}$$

Theorem 2 If Assumptions 1-3 hold, $y_{\varepsilon}^{*}(k_{i+1}) = const$, $\alpha_a > \alpha_{amin}$ with $\alpha_{amin} = \frac{b^2(K_{pa}+\frac{K_a}{T_s})^2}{4}$, $\alpha_c > \alpha_{cmin}$ with $\alpha_{cmin} = \frac{b^2(K_{pa}+\frac{K_a}{T_s})^2}{2}$, $\sigma_a \in (0,1]$, $\sigma_c \in (0,1]$, $\eta_a \in (0,1]$, $\eta_c \in (0,1]$, $\mu_a > 0$, and $\mu_c > 0$, the output tracking error of the system is asymptotically convergent.

Proof 2 The following is an example of a proof of the elevation angle control law $V_1(k)$. The proofs for the heading angle and the pitch angle are similar. Define the estimation error as $\tilde{\phi}_a(k) = \hat{\phi}_a(k) - \phi_a(k)$, we have

$$\begin{aligned}
\tilde{\phi}_a(k) =& \hat{\phi}_a(k-1) + \frac{\eta_a \Delta u_a(k-1)}{\mu_a + (\Delta u_a(k-1))^2} \times (\Delta y_\varepsilon(k) - \hat{\phi}_a(k-1)\Delta u_a(k-1)) - \phi_a(k) \\
=& \tilde{\phi}_a(k-1) - \frac{\eta_a \Delta u_a(k-1)}{\mu_a + (\Delta u_a(k-1))^2} \times (\tilde{\phi}_a(k-1)\Delta u_a(k-1)) - \Delta\phi_a(k) \\
=& \left(1 - \frac{\eta_a \Delta u_a(k-1)^2}{\mu_a + (\Delta u_a(k-1))^2}\right) \tilde{\phi}_a(k-1) - \Delta\phi_a(k)
\end{aligned} \tag{27}$$

Next, absolute values are taken on both sides of Equation (27). Then, we have

$$\begin{aligned}
\left|\tilde{\phi}_a(k)\right| \leq& \left|\left(1 - \frac{\eta_a \Delta u_a(k-1)^2}{\mu_a + (\Delta u_a(k-1))^2}\right) \tilde{\phi}_a(k-1)\right| + |\Delta\phi_a(k)| \\
\leq& \left|1 - \frac{\eta_a \Delta u_a(k-1)^2}{\mu_a + (\Delta u_a(k-1))^2}\right| \left|\tilde{\phi}_a(k-1)\right| + |\Delta\phi_a(k)|
\end{aligned} \tag{28}$$

where $\frac{\eta_a \Delta u_a(k-1)^2}{\mu_a + (\Delta u_a(k-1))^2}$ is monotonically increasing with respect to $\Delta u_a(k-1)^2$. Its minimum value is $\frac{\eta_a \epsilon^2}{\mu_a + \epsilon^2}$. When $0 < \eta_a \leq 1$ and $\mu_a > 0$, there exists a constant d_a that satisfies

$$\left|1 - \frac{\eta_a \Delta u_a(k-1)^2}{\mu_a + (\Delta u_a(k-1))^2}\right| \leq 1 - \frac{\eta_a \epsilon^2}{\mu_a + \epsilon^2} \triangleq d_a < 1 \tag{29}$$

From Lemma 1, we have

$$\begin{aligned}
\left|\tilde{\phi}_a(k)\right| \leq& d_a \left|\tilde{\phi}_a(k-1)\right| + 2b \\
\leq& d_a^2 \left|\tilde{\phi}_a(k-2)\right| + 2b(d_a+1) \\
\leq& \cdots \\
\leq& d_a^{k-1} \left|\tilde{\phi}_a(1)\right| + 2b \frac{1 - d_a^{k-1}}{1 - d_a}
\end{aligned} \tag{30}$$

Define $e_\varepsilon(k_i)$ as the tracking error of the output $y_\varepsilon(k_i)$. Since the event is not triggered, we have $e_\varepsilon(k+1) \approx e_\varepsilon(k)$. Moreover, it is useful to consider successive triggered moments k_{i-1}, k_i, and k_{i+1}. Substituting Equation (2) into $e_\varepsilon(k_{i+1})$ and applying Equation (23), we have

$$\begin{aligned}
e_\varepsilon(k_{i+1}) &= y_\varepsilon^*(k_{i+1}) - y_\varepsilon(k_{i+1}) \\
&= y_\varepsilon^*(k_{i+1}) - y_\varepsilon(k_i) - \Delta y_\varepsilon(k_{i+1}) \\
&= y_\varepsilon^*(k_{i+1}) - y_\varepsilon(k_i) - (K_{pa} + \frac{K_a}{T_s}) \frac{\sigma_a \phi_a(k_i)\hat{\phi}_a(k_i)}{\alpha_a + \left|\hat{\phi}_a(k_i)\right|^2} (y_\varepsilon^*(k_{i+1}) - y_\varepsilon(k_i)) \\
&\quad + \frac{K_a}{T_s} \frac{\sigma_a \phi_a(k_i)\hat{\phi}_a(k_{i-1})}{\alpha_a + \left|\hat{\phi}_a(k_{i-1})\right|^2} (y_\varepsilon^*(k_i) - y_\varepsilon(k_{i-1})) \\
&= \left[1 - \left(K_{pa} + \frac{K_a}{T_s}\right) \frac{\sigma_a \phi_a(k_i)\hat{\phi}_a(k_i)}{\alpha_a + \left|\hat{\phi}_a(k_i)\right|^2}\right] e_\varepsilon(k_i) + \frac{K_a}{T_s} \frac{\sigma_a \phi_a(k_i)\hat{\phi}_a(k_{i-1})}{\alpha_a + \left|\hat{\phi}_a(k_{i-1})\right|^2} e_\varepsilon(k_{i-1}) \\
&= B_a(k_i)e_\varepsilon(k_i) + C_a(k_i)e_\varepsilon(k_{i-1})
\end{aligned} \tag{31}$$

Table 1. The parameters of the controlled helicopter

Parameters	Values
DC motor voltage of the front and back motors V_f, V_b	$[-24, +24]$ V
Propeller force-thrust constant K_f	0.1188 N/V
Distance L_a	0.66 m
Distance L_h	0.178 m
Equivalent gravitational moment T_g	0.6108 N
Moment of inertia about elevation J_x	1.0348 kg · m²
Moment of inertia about heading J_y	0.0451 kg · m²
Moment of inertia about pitch J_z	1.0348 kg · m²

If $\alpha_a > \alpha_{amin}$ with $\alpha_{amin} = \frac{b^2(K_{pa}+\frac{K_a}{T_s})^2}{4}$ and $\sigma_a \in (0, 1]$, and there exist constants $M_{a1} \in (0, 1)$ and $M_{a2} \in (0, 1)$ such that

$$0 < M_{a1} < \frac{K_a}{T_s}\frac{\sigma_a\phi_a(k_i)\hat{\phi}_a(k_{i-1})}{\alpha_a + \left|\hat{\phi}_a(k_{i-1})\right|^2} < \frac{K_a}{T_s}\frac{\sigma_a b}{2\sqrt{\alpha_a}} \leq \frac{K_a}{K_{pa}T_s + K_a}\sigma_a < \sigma_a \leq 1 \tag{32}$$

$$0 < M_{a2} < \left(K_{pa} + \frac{K_a}{T_s}\right)\frac{\sigma_a\phi_a(k_i)\hat{\phi}_a(k_i)}{\alpha_a + \left|\hat{\phi}_a(k_i)\right|^2} < \frac{K_a}{K_{pa}T_s + K_a}\frac{\sigma_a b}{2\sqrt{\alpha_a}} < \sigma_a \leq 1 \tag{33}$$

Hence, there exist constants b_{a1} and b_{a2} such that $|B_a(k_i)| < |1 - M_{a2}| \triangleq b_{a1} < 1$, and $|C_a(k_i)| < b_{a2} < 1$. Taking absolute values for both sides of Equation (31) yields

$$\begin{aligned} |e_\varepsilon(k_{i+1})| &\leq b_{a1}\,|e_\varepsilon(k_i)| + b_{a2}\,|e_\varepsilon(k_{i-1})| \\ &\leq b_{a1}\,|b_{a1}\,|e_\varepsilon(k_{i-1})| + b_{a2}\,|e_\varepsilon(k_{i-2})|| + b_{a2}\,|b_{a1}\,|e_\varepsilon(k_{i-2})| + b_{a2}\,|e_\varepsilon(k_{i-3})|| \\ &\leq \cdots \\ &\leq \left(b_{a1}^{k_i} + b_{a1}b_{a2}^{k_{i-1}} + b_{a2}b_{a1}^{k_{i-1}} + b_{a2}^{k_i}\right)|e_\varepsilon(1)| \end{aligned} \tag{34}$$

In summary, $e_\varepsilon(k_i)$ eventually converges to the set $(b_{a1} + b_{a2})\,|e_\varepsilon(1)|$. Since $e_\varepsilon(k_{i+1}) = y_\varepsilon^*(k_{i+1}) - y_\varepsilon(k_{i+1})$ and $y_\varepsilon^*(k_{i+1}) = const$, it is obtained that $y_\varepsilon(k_{i+1})$ is bounded.

During the event-triggered interval (k_{i-1}, k_i), the control signal retains its value from the last event-triggered instant. If the tracking error exceeds the event-triggered threshold value, defined in Equation (22), the controlled plant will enter event-triggering phases.

Based on the above analysis, Theorem 2 is proved.

5. SIMULATION STUDIES

In this section, the MATLAB/Simulink software is employed to verify the validity of the designed control scheme. Referring to [45], the structural diagram of the three-degree-of-freedom helicopter is shown in Figure 5, where the corresponding parameters are listed in Table 1 [45].

In simulation, the sampling time is set to $T_s = 0.1$s. The initial values are set as $\hat{\phi}_a(1) = \hat{\phi}_{c1}(1) = \hat{\phi}_{c2}(1) = 0.5$, $u_a(1) = 0$, and $u_c(1) = 0$. The parameters of the designed method are set as $\eta_a = 1.5$, $\mu_a = 1$, $\sigma_a = 1$, $\alpha_a = 1$, $\eta_c = 1$, $\mu_c = 2$, $\sigma_c = 0.6$, and $\alpha_c = 1$. According to Lemma 3, we choose $\varphi = 0.5$, $\nu = 20$, $\upsilon(1) = 1$, $\omega = 1e^{-3}$, and $\varphi + \frac{1}{\nu} = 0.5 + \frac{1}{20} = 0.55 \in (0, 1)$. Selecting $a_1 = 0.9$ and $a_2 = 1.4$, we have $\tau_a < 4.19$. Then, letting $\tau_a = 4$ and $\upsilon_0 = 0$, it is obtained that $|\upsilon_a(0, 24)| < 6$.

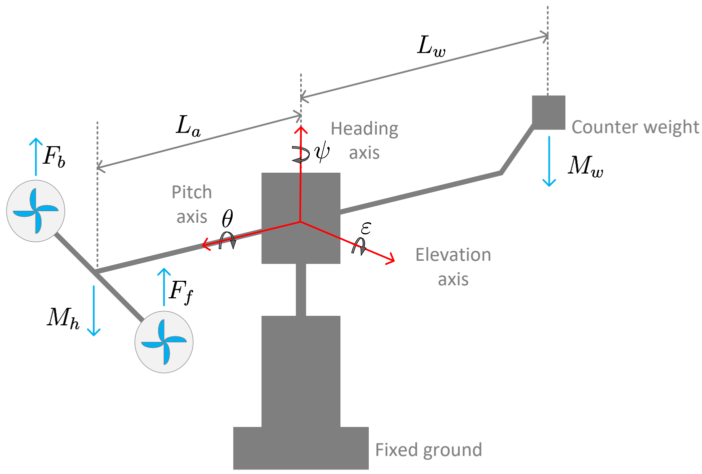

Figure 5. Structural diagram of a three-degree-of-freedom helicopter.

5.1. Time-invariant angle tracking

Here, the three attitude angles are set as $\varepsilon^* = 0.6$, $\psi^* = 0.6$, and $\theta^* = 0$. The designed method is evaluated by comparing it with the existing method [40]. Figure 6A-C presents the simulation results of elevation, heading, and pitch channel, respectively. Figure 6D is the event-triggered interval for the elevation angle of the developed method. Figure 6E shows the simulation results of the elevation angle under different DoS attack intensities.

As shown in Figure 6A-C, the proposed method enables the helicopter system to efficiently track the desired angles by adjusting the control inputs in real-time, even under aperiodic DoS attacks. It should be pointed out that the gray bars denote the successive DoS attacks, as shown in Figure 6A-C. The designed method is effective against successive DoS attacks. Figure 6A shows that the dynamic event triggering strategy provides a slight improvement in response speed compared to the static event triggering strategy. Figure 6B and C illustrates that the dynamic event triggering strategy reduces overshooting by a greater amount than the static event triggering strategy. Figure 6D indicates that the dynamic event triggering strategy reduces the communication resources by 63.47%, while the static event triggering strategy reduces them by only 54.8%. This indicates that the dynamic event-triggering strategy can further reduce communication resources and load. Figure 6E demonstrates that the convergence rate slows down as the intensities of DoS attacks gradually increase.

Remark 8 To further validate the real-time potential of the proposed control method, the controller was deployed on a remote computer. The hardware configuration of the remote computer is as follows: it is equipped with an Intel Core i5-9300H processor (base frequency 2.4 GHz, maximum turbo frequency 4.1 GHz, four cores and eight threads), two 8GB DDR4 memories (frequency 2,666 MHz), and an NVIDIA GeForce GTX 1650 graphics card. By executing a 50,000-step simulation test, the average runtime per step was found to be 4.416 us.

5.2. Time-varying angle tracking

The desired angle of the elevation channel is set as $\varepsilon^* = 0.6\sin(0.5t)$, however, other angles are set the same as the time-invariant example. Selecting $\beta = 0.5$, the control results of different DoS compensations are shown in Figure 7. Figure 7A-C presents the simulation results of elevation, heading, and pitch angles, respectively. Figure 7D is the event-triggered interval of the proposed method and the existing method [44]. From Figure 7A-C, the proposed algorithm enables the helicopter system to efficiently track the time-varying target angle under

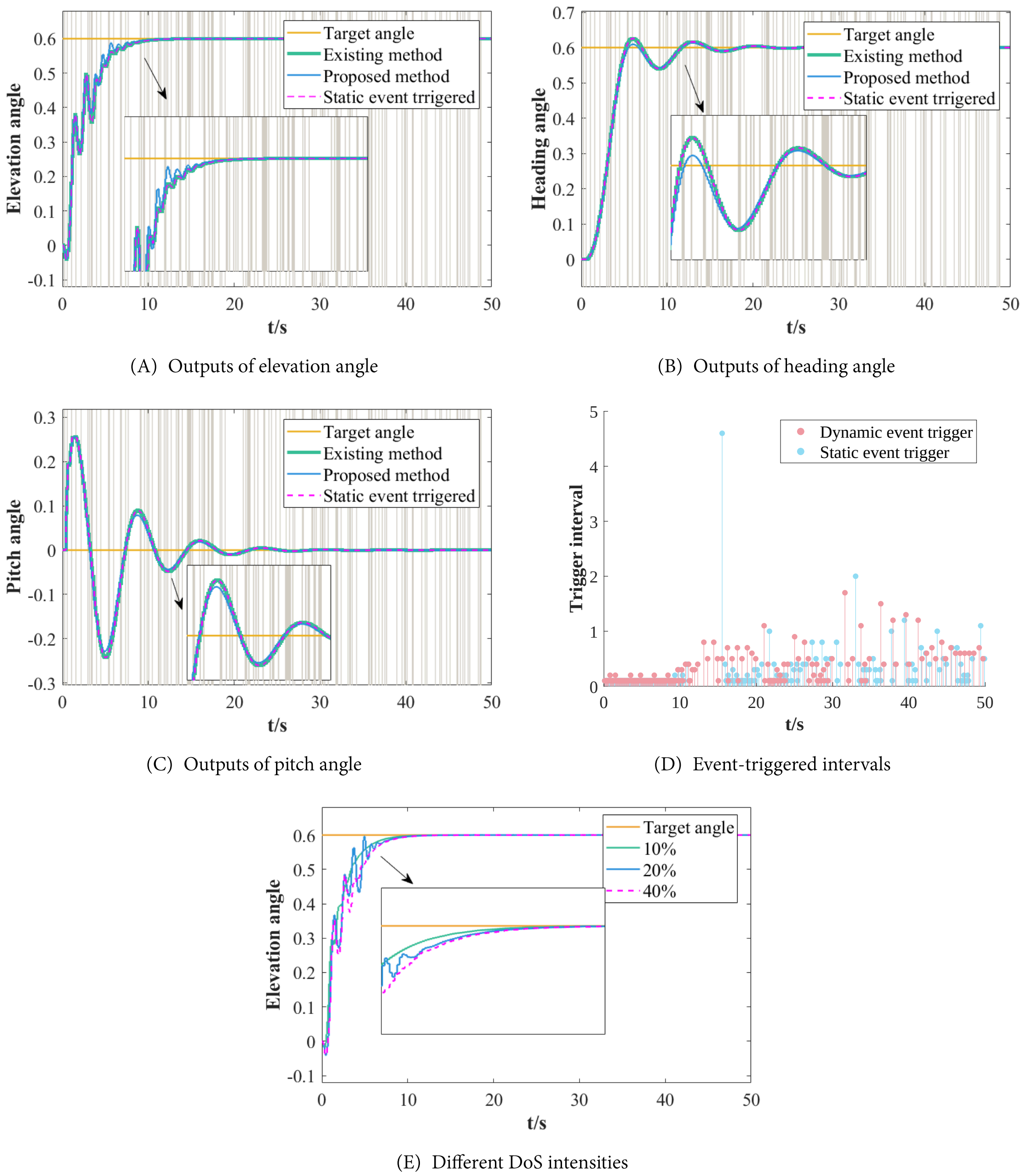

Figure 6. Time-invariant angle tracking. DoS: Denial-of-service.

aperiodic DoS attacks. Meanwhile, it can be seen from Figure 7A that the elevation angle possesses a faster convergence rate, from Figure 7B that the heading angle possesses a smaller overshoot and a faster convergence rate, and from Figure 7C that the pitch angle possesses a faster convergence rate.

5.3. Parametric analysis

The results of the parameter analysis are shown in Figure 8, where the parameters involved in this section are tuned individually, and the other parameters are consistent with the time-invariant angle tracking experiment. First, the parameter w is analyzed, and the results are shown in Figure 8A. As the event-triggered threshold w is changed from 10^{-5} to 10^{-2}, the event-triggered frequency decreases obviously. However, once the event-triggered threshold w continues to grow larger than 10^{-2}, the system will not be able to track the desired

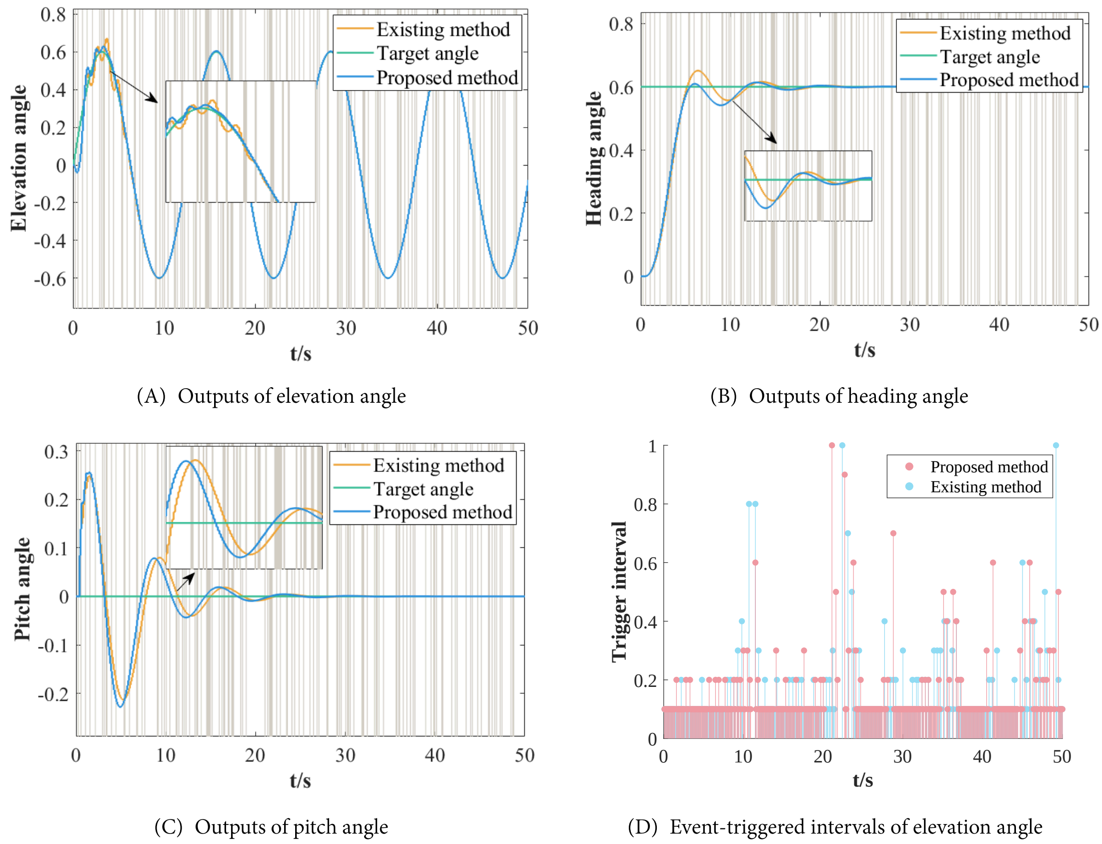

(A) Outputs of elevation angle

(B) Outputs of heading angle

(C) Outputs of pitch angle

(D) Event-triggered intervals of elevation angle

Figure 7. Time-varying angle tracking.

angle accurately, and the event-triggered frequency increases rapidly instead. Therefore, the user can balance communication costs and control performance by selecting the value of the parameter.

Then, as shown in Figure 8B, the parameter K_{pa} is analyzed. When K_{pa} gradually increases from 1.5 to 1.8, the event-triggered interval decreases from 260 to around 210. However, when K_{pa} increases from 1.8 to 2.0, the event-triggered interval oscillates rather than gradually decreases. After that, as K_{pa} continues to increase, the event-triggered interval decreases rapidly.

6. CONCLUSIONS

This paper proposed a dynamic event-triggered model-free adaptive attitude control method for a three-degree-of-freedom helicopter with aperiodic DoS attacks. First, the outputs were redefined as a linear combination of angles and angular velocities, effectively solving the quasi-linearization requirements issue. Moreover, a dynamic event-triggered scheme has been developed. Compared with the existing scheme, the designed mechanism further reduces the communication frequencies. In the future, we will further consider extending the central algorithm of the current framework to multi-helicopter systems by combining it with distributed communication and decision-making mechanisms, and build a hardware-in-the-loop simulation system to verify the real-time performance and reliability of the algorithms in a real hardware environment.

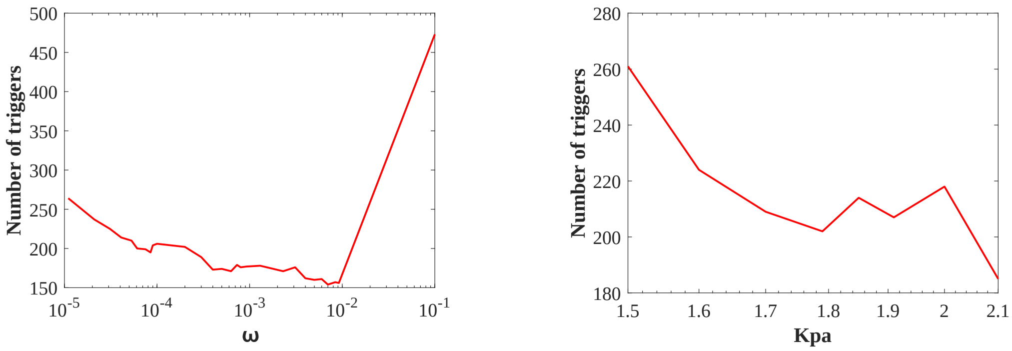

(A) Trigger count varies with ω (B) Trigger count varies with K_{pa}

Figure 8. Parametric analysis.

DECLARATIONS

Authors' contributions

Made substantial contributions to conception and design of the study and performed data analysis and interpretation: Xu, Y.; Zhao, H.

Performed data acquisition and provided administrative and technical support: Gao, Y.; Yu, H.; Peng, L.

Availability of data and materials

The original contributions presented in this study are included in the article.

Financial support and sponsorship

This work was supported in part by the National Natural Science Foundation of China (62403216), in part by the Basic Research Program of Jiangsu Province (BK20241608), in part by the Wuxi Science and Technology Development Fund Project (K20231015), in part by the Wuxi Young Science and Technology Talent Support Program (TJXD-2024-114), in part by the 111 Project (B23008), and in part by the EU iMARs Project (HORIZON-MSCA-2023-101182996).

Conflicts of interest

All authors declared that there are no conflicts of interest.

Ethical approval and consent to participate

Not applicable.

Consent for publication

Not applicable.

REFERENCES

1. Huang, J.; Yu, T.; Zhu, X.; et al. Energy efficiency maximization in UAV-assisted intelligent autonomous transport system for 6G networks with energy harvesting. *IEEE Trans. Intell. Transp. Syst.* **2024**, 1-11. DOI
2. Sun, G.; He, L.; Sun, Z.; et al. Joint task offloading and resource allocation in aerial-terrestrial UAV networks with edge and fog computing for post-disaster rescue. *IEEE Trans. Mob. Comput.* **2024**, *23*, 8582–600. DOI
3. Pan, L.; Song, C.; Gan, X.; Xu, K.; Xie, Y. Military image captioning for low-altitude UAV or UGV perspectives. *Drones* **2024**, *8*, 421. DOI
4. Zhao, T.; Li, W. *LQR*-based attitude controllers design for a 3-DOF helicopter system with comparative experimental tests. *Int. J. Dynam.*

Control **2024**, *12*, 1063–72. DOI
5. Pandey, V.; Kamal, S.; Ghosh, S. Finite-time discrete control for two-DOF helicopter system. *IEEE Trans. Circuits Syst. II Exp. Briefs* **2024**, *71*, 3800–4. DOI
6. Mokhtari, M. A. Adaptive neural network-based dynamic surface control for a 3-DoF helicopter. *J. Control Autom. Electr. Syst.* **2024**, *35*, 326–36. DOI
7. Wang, C.; Li, W.; Liang, M. Event-triggered prescribed performance adaptive fuzzy fault-tolerant control for quadrotor UAV with actuator saturation and failures. *IEEE Trans. Aerosp. Electron. Syst.* **2025**, *61*, 813–28. DOI
8. Soleimani, E.; Sedigh, A. K.; Nikoofard, A. Data-driven reinforcement learning-based forgetting factor iterative learning control. *IEEE Trans. Autom. Sci. Eng.* **2025**, *22*, 12245–56. DOI
9. Shi, H.; Chen, Q.; Hong, Y.; Ou, X.; He, X. Adaptive fuzzy iterative learning control of constrained systems with arbitrary initial state errors and unknown control gain. *IEEE Trans. Autom. Sci. Eng.* **2025**, *22*, 6439–50. DOI
10. Cui, L.; Chakraborty, S.; Ozbay, K.; Jiang, Z. P. Data-driven combined longitudinal and lateral control for the car following problem. *IEEE Trans. Control Syst. Technol.* **2025**, *33*, 991–1005. DOI
11. Xia, Z.; Dai, X.; Li, Y.; Wang, L.; Chen, F.; Ma, J. A data-driven control method for nonlinear characteristics of variable frequency regulation for wide-distance-range adaptive WPT system. *IEEE Trans. Power Electron.* **2025**, *40*, 10221–41. DOI
12. Hou, Z.; Huang, W. The model-free learning adaptive control of a class of SISO nonlinear systems. In *Proceedings of the 1997 American Control Conference (Cat. No.97CH36041)*, Albuquerque, USA. June 06-06, 1997. IEEE; 1997. pp. 343-4. DOI
13. Liu, L.; Han, X.; Fan, H.; Liu, L.; Wang, B. Model-free adaptive control of the combined aircraft with unknown multi-source disturbances and output saturation. *Aerosp. Sci. Technol.* **2025**, *165*, 110471. DOI
14. Yu, Q.; Wu, S.; Bu, X.; Hou, Z. Model free adaptive predictive iterative learning cooperative control of multiple high-speed trains operation with disturbances. *IEEE Trans. Autom. Sci. Eng.* **2025**, *22*, 19929-44. DOI
15. Ding, H.; Shen, H.; Park, J. H.; Xie, Q. Model free adaptive control of strip temperature in continuous annealing furnace based on quantum-behaved particle swarm optimization. *Nonlinear Dyn.* **2025**, *113*, 629–43. DOI
16. Liu, S.; Yan, Y.; Ren, Y.; Jin, S.; Hou, Z. Attitude adjustment of a two-wheel balance vehicle based on an enhanced model-free adaptive control algorithm. *IEEE Trans. Circuits Syst. II Exp. Briefs* **2024**, *71*, 3885–9. DOI
17. Liu, L.; Zhang, Z.; Zhao, Y.; et al. Data-driven model-free adaptive control for power converter under multiscenarios in microgrids. *IEEE Trans. Ind. Electron.* **2025**, *72*, 8060-71. DOI
18. Ding, Y.; Wang, J.; Zhang, J.; Luo, X. Design of quadcopter attitude controller based on data-driven model-free adaptive sliding mode control. *Int. J. Dynam. Control* **2024**, *12*, 1404–14. DOI
19. Xin, L.; He, G.; Long, Z. Stealthy false data injection attacks detection and classification in cyber-physical systems using deep reinforcement learning. *IEEE Trans. Autom. Sci. Eng.* **2024**, *22*, 141–53. DOI
20. Guo, J.; Zhang, Q.; Zhao, Y. Identification of FIR systems with binary-valued observations under replay attacks. *Automatica* **2025**, *172*, 112001. DOI
21. Zhao, H.; Zhao, Z.; Xu, D.; Yu, H. Event-triggered automatic parking control for unmanned vehicles against DoS attacks. *IEEE Trans. Ind. Cyber Phys. Syst.* **2024**, *2*, 531–41. DOI
22. Xiong, H.; Chen, G.; Ren, H.; Li, H. Broad-learning-system-based model-free adaptive predictive control for nonlinear MASs under DoS attacks. *IEEE/CAA J. Autom. Sinica* **2025**, *12*, 381–93. DOI
23. Ma, Y. S.; Che, W. W.; Deng, C.; Wu, Z. G. Distributed model-free adaptive control for learning nonlinear MASs under DoS attacks. *IEEE trans. Neural Netw. Learn. Syst.* **2021**, *34*, 1146–55. DOI
24. Li, Y.; Li, X. Improved nonlinear model-free adaptive iterative learning control in DoS attack environment. *IET Control Theory Appl.* **2024**, *18*, 825–33. DOI
25. Moloudian, G.; Hosseinifard, M.; Kumar, S.; et al. RF energy harvesting techniques for battery-less wireless sensing, industry 4.0, and internet of things: a review. *IEEE Sens. J.* **2024**, *24*, 5732–45. DOI
26. Dou, Y.; Xing, G.; Ma, A.; Zhao, G. A review of event-triggered consensus control in multi-agent systems. *J. Control Decis.* **2025**, *12*, 1–23. DOI
27. Pang, Y.; Zhuang, G.; Xia, J.; Xie, X. Fault detection and robust security control for implicit jump systems against random FDI attacks and packet loss under memorized output-perceptive event-triggered protocol. *IEEE Trans. Inf. Forensics Secur.* **2024**, *19*, 7362–73. DOI
28. Liu, X.; Qiu, L.; Fang, Y.; Wang, K.; Li, Y.; Rodríguez, J. A two-step event-triggered-based data-driven predictive control for power converters. *IEEE Trans. Ind. Electron.* **2024**, *71*, 13545–55. DOI
29. Yu, J.; Ma, Z.; Li, K.; Chang, M. Event-triggered control of lag consensus for leader-following multi-agent systems with nonlinear dynamics. *Circuits Syst. Signal Process.* **2024**, *43*, 3500–15. DOI
30. Liu, J.; Xu, C.; Li, S.; Dong, Z.; Hu, X. Event-triggered ADRC-MFAC for intelligent tugs in escort operations with a thrust re-allocation strategy. *Control Eng. Pract.* **2025**, *156*, 106237. DOI
31. You, X.; Xiao, K.; Wang, G. A static event-triggered background-impulse kalman filter for wireless sensor networks with non-Gaussian measurement noise. *Inf. Fusion* **2025**, *118*, 102955. DOI
32. Wen, Q.; Zhang, J.; Fan, H.; Liu, L.; Wang, B. Review on application of model-free adaptive control in flight control systems. *Tact. Miss. Technol.* **2024**, *4*, 41–52+91. https://caod.oriprobe.com/articles/67668280/wu_mo_xing_zi_shi_ying_kong_zhi_zai_fei_xing_kong_.htm. (accessed 9 Sep 2025)
33. Hou, Z.; Jin, S. A novel data-driven control approach for a class of discrete-time nonlinear systems. *IEEE Trans. Control Syst. Technol.* **2010**, *19*, 1549–58. DOI

34. Hou, Z.; Jin, S. Model free adaptive control. 1st edition. CRC press Boca Raton, FL, USA; 2013. DOI
35. Chang, L.; Chi, R.; Hou, Z. Coding-decoding protocol-based data-driven adaptive sliding mode control under energy-constrained DoS attacks. *IEEE Trans. Autom. Sci. Eng.* **2025**, *22*, 16668–81. DOI
36. Zhou, Q.; Ren, Q.; Ma, H.; Chen, G.; Li, H. Model-free adaptive control for nonlinear systems under dynamic sparse attacks and measurement disturbances. *IEEE Trans. Circuits Syst. I Regul. Pap.* **2024**, *71*, 4731–41. DOI
37. Bu, X.; Yu, W.; Yu, Q.; Hou, Z.; Yang, J. Event-triggered model-free adaptive iterative learning control for a class of nonlinear systems over fading channels. *IEEE Trans. Cybern.* **2022**, *52*, 9597–608. DOI
38. Liu, S.; Lin, G.; Ji, H.; Jin, S.; Hou, Z. A novel enhanced data-driven model-free adaptive control scheme for path tracking of autonomous vehicles. *IEEE Trans. Intell. Transp. Syst.* **2024**, *26*, 579–90. DOI
39. Zhang, C.; Cen, C.; Huang, J. An overview of model-free adaptive control for the wheeled mobile robot. *World Electr. Veh. J.* **2024**, *15*, 396. DOI
40. Wang, J.; Wang, X.; Wang, X.; Zhang, Z.; Wang, J. Model free adaptive attitude control for a 3-DOF helicopter. *IET Control Theory Appl.* **2023**, *40*, 2295-303. DOI
41. Zhao, H.; Xu, D.; Zhou, Z.; Yu, H. Dynamic event-triggered resilient heading control for unmanned surface vehicle with encrypted data. *IEEE Trans. Intell. Veh.* **2024**, *9*, 5718–27. DOI
42. Ma, Y. S.; Che, W. W.; Deng, C. Dynamic event-triggered model-free adaptive control for nonlinear CPSs under aperiodic DoS attacks. *Inform. Sci.* **2022**, *589*, 790–801. DOI
43. Liao, Y.; Jiang, Q.; Du, T.; Jiang, W. Redefined output model-free adaptive control method and unmanned surface vehicle heading control. *IEEE J. Ocean. Eng.* **2020**, *45*, 714–23. DOI
44. Pang, Z. H.; Liu, G. P.; Zhou, D.; Sun, D. Data-driven control with input design-based data dropout compensation for networked nonlinear systems. *IEEE Trans. Control Syst. Technol.* **2016**, *25*, 628–36. DOI
45. Castañeda, H.; Plestan, F.; Chriette, A.; de León-Morales, J. Continuous differentiator based on adaptive second-order sliding-mode control for a 3-DOF helicopter. *IEEE Trans. Ind. Electron.* **2016**, *63*, 5786–93. DOI